GRAPE SEED CARBONS FOR STUDYING THE INFLUENCE OF TEXTURE ON SUPERCAPACITORBEHAVIOUR IN AQUEOUS ELECTROLYTES

Diana Jiménez-Cordero[a,b], Francisco Heras[a], Miguel A. Gilarranz[a], Encarnación Raymundo-Piñero[b,c].*

[a]S.D. Ingeniería Química, Universidad Autónoma de Madrid. Ctra. Colmenar Viejo, km 15. 28049 Madrid (Spain)

[b]Centre de Recherche sur la Matière Divisée, CNRS University, 1b Rue de la Férollerie, 45071 Orléans, France.

[c]CNRS, CEMHTI UPR3079, Univ. Orléans, F-4071 Orléans, France.

Abstract

Microporous carbon materials having a negligible contribution of mesopores have been synthesized by cyclic oxidation/desorption of grape seeds char using air, ozone and HNO_3 as oxidant agents. By adequate selection of the operating conditions (oxidation procedure and number of cycles) it is possible to tune the volume and pore size distribution of carbon materials and therefore determine the influence of carbon textural properties on the electrochemical behaviour of carbon-carbon symmetric supercapacitors operating in different aqueous electrolytes. The results confirm that although energy density can be improved using neutral electrolytes in reason of their higher stability potential window compared to acidic or basic ones, it is important to adapt the textural properties of the carbon materials to improve the ions diffusion inside

* Corresponding author Tel.: +34 914978051; fax: +34 914972981.

  E-mail address: fran.heras@uam.es

the porosity for assuring the charging of the double layer at high current densities to reach high power densities.

1. Introduction

Electric double-layer capacitors (EDLC), often known as "supercapacitors", have recently received much attention in high power electrochemical technology research. The behavior of double-layer charging at the distributed interface of high specific surface materials – such as activated carbon (AC) powders, carbon nanotubes (CNT)or carbon gels, fullerenes, etc. - has been widely studied [1].

The energy storage mechanism in supercapacitor is based on an electrostatic attraction between charges along the double layer formed at the electrode/electrolyte interface. Since this phenomenon is controlled by the surface area of the interface, ACs are the most extensively used electrode materials for EDLC.In addition to their high specific surface area (SSA), ACs have other advantages such as availability, easy process ability and relatively low cost of most of precursors and production technologies [2, 3]. To usethese materials as electrodes for supercapacitors certain conditions are needed, such as a high conductivity ensuring a high power density, and an adequate pore size distribution (PSD), mainly with an average pore size smaller than 1nm. Moreover, a large quantity of surface functionalities can be a source of additional capacitance, called pseudo-capacitance, as some particular functionalities could undergo fast redox reactions with the electrolyte when working in aqueous solutions such as H_2SO_4 or KOH [4].

When a supercapacitor is connected to a voltage source, the surface of the electrodes is charged and attracts the ions of opposite charge. The ions are stored at the surface of

electrodes. The sizes of ions and pores and the type of connection between the pores and the outer surface of the carbon particles may also strongly influence the values of capacitance, especially under high operating current densities. Li et al. 2011 [5] used a biomass residue (sunflower seed shell) as precursor for nanoporous activated carbon to prepare electrodes in electric double-layer capacitors working with KOH as aqueous electrolyte and they obtained interesting results with maximum values for specific capacitance, energy density and power density of $35\mu Fcm^{-2}$, $6WhKg^{-1}$ and $60KWKg^{-1}$. Raymundo-Piñero et al. [3] have studied the effect of pore size in aqueous and organic electrolytes using a series of porous carbons prepared from the same precursor, texturally identical and only differing in their average pore width. They obtained maximum values of specific capacitance of 15.9 μFcm^{-2} using KOH as electrolyte and found that the gravimetric capacitances of these carbons increase as the average micropore size (L_0) decreases, resulting that not only the SSA but also the porous nanotexture of carbons must be seriously taken into account for understanding their capacitance properties. Similar results have been obtained by Chmiola et al. by using carbide derived carbons (CDC) in organic electrolytes or ionic liquids with maximum values of specific capacitance of 13.5 μFcm^{-2}[6].Guo et al. 2003[7] prepared high specific surface area AC from rice husks and studied different activation conditions leading to different pore structures of the carbons, in order to study how they affect their electrochemical behavior. These authors found that the specific capacitance (maximum value of $12.9\mu Fcm^{-2}$) was not proportional to the SSA and samples with wider mesopore gave the lowest capacitance, thus showing that the capacitance of a porous carbon is strongly dependent on the pore structure. Moreover, Yang et al. 2008 [8], using walnut shells nanoporous AC, obtained by means of simultaneous physical–chemical activation, confirmed that porestructure, especially pore size distribution, has a

significant influence on the performance of supercapacitors. They obtained maximum values for specific capacitance, energy density and power density of 24.1 μFcm^{-2}, 7.3WhKg^{-1} and 770WKg^{-1} using KOH as electrolyte. Markoulidis et al. 2013 [9] studied the performance of supercapacitors cells with AC adding multiwall carbon nanotubes (MWCNTs) – from peat bog-derived charcoal – in organic electrolytes and they found that the MWCNT improve the efficiency of supercapacitors leading to maximum values of specific capacitance, energy density and power density of 21.6μFcm^{-2}, 28WhKg^{-1} and 38KWKg^{-1}.

The above cited studies were performed for supercapacitors operating in organic electrolytes or in acid or basic aqueous solutions. Recently, it has been shown that supercapacitors using neutral electrolytes outperform the other aqueous electrolytes based ones in terms of cell voltage and energy density [10-12].They are an environmentally friendly alternative to the commercialized supercapacitors using organic electrolytes as they present comparable electrochemical performances in terms of energy density. Nevertheless, a deeper study regarding the influence of the carbon based electrodes textural properties on the electrochemical capacitance of those supercapacitors will be of a great interest.

Indeed, tailoring the porous structure of carbon materials for a given electrolyte is a major goal of supercapacitors optimization [13]. In this sense, an activation method by cycles of oxygen chemisorption-desorption has been proposed for a controlled activation of carbonaceous precursors that allows to achieve a targeted porosity development [14, 15]. This method consists of an oxidation step at low temperature followed by desorption of chemisorbed oxygen (as carbon oxides) in inert atmosphere at high temperature. The purpose of the oxidation step in the cyclic activation method is the uptake of oxygen by the AC that can then be released as CO/CO_2 in the subsequent

desorption stage, thus leading to porosity development [16]. The sequence is repeated until convenient porosity development is achieved [17].

In this work, three series of ACs obtained by cyclic activation from grape seeds char, with different textural properties and pore size distribution, were evaluated. The influence of these different carbon features on the electrochemical behavior has been explored in a neutral aqueous electrolyte as 1 molL^{-1} Na$_2$SO$_4$. The differences found when using acid and basic aqueous electrolytes i.e. 1 molL^{-1} H$_2$SO$_4$, 6 molL^{-1} KOH are discussed.

2. Experimental

2.1 Materials

The raw material used in this study were seeds from grapes of the variety "Tinta de Toro" harvested, for red wine manufacture, in the city of Toro (Spain). The seeds were washed, dried and then were extracted to remove oil using hexane in a Soxhlet apparatus before pyrolysis. The char used as a starting material in the activation process was obtained by flash pyrolysis of the extracted seeds at 800ºC, determined as the optimum temperature in previous works [18]. The pyrolysis char yield was 34 % (w, extracted seeds dry basis).

Three series of ACs from the char obtained were prepared by cyclic oxidation-desorption using three different oxidation procedures (A: air, O: ozone, N: nitric acid). In A and O series gas phase oxidation was employed, using air (21% oxygen) and ozone (300mg h^{-1}in air flow of 50mLmin^{-1}STP) as activating agents[15, 19]. The oxidation step of each cycle was carried out at 275ºC for 2h and a gas flow of 100mLmin^{-1}STP,

5

while the desorption step was carried out at 850ºC for 2h under a flow rate of 100 mLmin^{-1}STP of nitrogen. The switch from oxidation to desorption step was carried out at a heating rate of 10ºCmin^{-1} under nitrogen flow. For the N series a liquid phase oxidation was employed using boiling HNO_3 (30%, v) under reflux for 20min. After oxidation, the samples were washed with distilled water until neutrality and dried in a muffle furnace at 105ºC. The desorption step was carried out at same conditions as gas phase oxidation series (850ºC, 2h and 100mLmin^{-1}STP N_2 flow) [20]. For all experimental conditions, 1 to 10 activation cycles were performed in each series.

The ACs were designated by the series and the number of cycles applied, e.g. A5 means the AC sample activated during 5 cycles using air oxidation.

2.2. Chemical and Textural Characterization

The composition of chars was analyzed by elemental analysis with a LECO VTF-900 apparatus and by X-ray photoelectron spectroscopy (XPS) with a VG ESCALAB 250.

Surface area and total pore volume of the samples were measured in an automated volumetric gas adsorption apparatus (MicromeriticsTristar 3020) by adsorption of N_2 at 77K and CO_2 at 273K. Approximately 0.15g of sample was used in each adsorption test. Samples were placed in a glass container and degassed at 150ºC during 7h prior to the adsorption measurements using a degas system (MicromeriticsVacPrep 061). The surface area (S_{BET}) of the samples was calculated from N_2 isotherms using Brunauer-Emmett-Teller equation [21] and the t-method was used to obtain the micropore volume ($V_{microN2}$, 0.9-2nm) and the BJH method to obtain the mesopore volume (V_{mesoN2}, 2-50nm), whereas Dubinin-Astakhov model was applied to CO_2 isotherms to determine surface area (S_{DA}) and the ultramicropore volume ($V_{microCO2}$, 0.4-0.9nm) [22]. The $V_{microN2}/V_T$ratio (where V_T is $V_{microN2} + V_{mesoN2}$) was used to assess the contribution of

micropores to the total pore volume. The non-local density functional theory (NLDFT) method was used to calculate both micropore and mesopore size distribution [23] and the average micropore width (L_0) was calculated by Stoeckli equation [24].

2.3. Electrochemical characterization

The electrodes used for the measurements were prepared by mixing the AC tested, powdered carbon black (PURE-BLACK Carbon, Superior Graphite Co.) as conductivity additive and a solution of Polytetrafluoroethylene (PTFE), used as a binder in a 8:1:1 ratio (%w) in the dry electrode. Ethanol was added to allow a good homogenization. The mixture was stretched to obtain a thin film and electrodes with 10mm diameter were cut and pressed to get 8-13mg pellets and a thickness of 300μm ± 50μm. The carbon pellets were dried in a muffle furnace at 120ºC to remove any humidity and ethanol. Two-electrode supercapacitor cells were assembled using two identical carbon pellets (electrodes), stainless steel current collectors, a porous membrane separator, and a Teflon Swagelok airtight system.

The electrochemical performance of the materials was evaluated in three aqueous electrolytes Na_2SO_4 $0.5molL^{-1}$, KOH $6molL^{-1}$ and H_2SO_4 $1molL^{-1}$ by cyclic voltammetry (CV) at $2mVs^{-1}$ and galvanostatic charge/discharge (GA) at first using $200mAg^{-1}$ in different range of maximum operating voltage: 0.6-2.0V for Na_2SO_4 and 0.6-1.4V for KOH and H_2SO_4, and later at a scan rate of $10mVs^{-1}$ with only one voltage value and a variable current density from 100mA to 30000mA using a multichannel potentiostat/galvanostat (Bio-Logic model VMP2).

The gravimetric capacitance (C) expressed in farads per gram of carbon material (Fg^{-1}) was estimated by the GA test. The specific surface capacitance Cs, expressed in farads per unit of SSA (μFcm^{-2}), was calculated as C/S_{BET}.

To obtain the electrical series resistance, ESR,(Ω) and the electrical distributed resistance, EDR (Ω), the impedance spectroscopy, in100kHz to 300mHz interval, was used by means of a VMP 2 device (Bio-Logic, France).

3. Results and Discussion

3.1. Chemical and textural characterization

The composition of char and ACs obtained after 1, 4, 7 and 10 activation cycles is summarized in Table 1. In spite of the fact that all series of samples were obtained from the same precursor, differences in composition of the ACs obtained were observed depending on the activating agent used. The carbon percentage profiles along the activation process were similar for the series activated in gas phase (A, O), showing a decrease with the activation cycles, especially for A10 sample, which shows the lower carbon mass fraction (52%). In contrast, the N series shows a higher carbon mass fraction increasing up to cycle 7 and decreasing from that point.

The oxygen mass fraction for the series activated in gas phase was higher, increasing along the cycles, while lower values and a decreasing profile were observed for the N series. The nitrogen mass fraction increased with the number of activation cycles applied for all series, although the values obtained were higher for the N series.

Respect to the minor elements, only in the case of the samples activated in gas phase where significant, being calcium, phosphorus and potassium the most relevant.

Table 1. Composition of char and ACs obtained by activation with air, ozone and HNO_3 after 1, 4, 7 and 10 activation cycles.

Sample	C (%)	H (%)	N (%)	S (%)	O (%)	P (%)	Ca (%)	K (%)	Ash and others (%)
Char	85.60	1.00	1.70	0.04	4.82	0.32	1.05	0.44	5.03
A1	79.85	0.65	1.46	0.00	4.40	0.42	1.15	0.00	12.07
A4	73.35	0.61	1.50	0.01	7.13	1.31	1.82	0.00	14.27
A7	71.38	0.57	1.65	0.03	6.85	--	--	--	19.52
A10	52.06	0.73	1.85	0.00	13.00	1.78	2.65	1.26	26.67
O1	79.69	0.65	1.44	0.00	4.47	0.78	1.49	1.49	9.99
O4	74.99	0.61	1.48	0.02	5.92	0.81	1.30	0.00	14.87
O7	72.49	0.70	1.57	0.02	7.07	0.76	1.15	0.03	16.21
O10	72.52	0.66	1.59	0.00	7.10	0.74	1.37	0.58	15.44
N1	82.48	0.59	1.81	0.00	4.13	0.67	0.77	0.44	9.11
N4	86.66	0.50	2.83	0.26	2.28	0.00	0.00	0.00	7.47
N7	88.42	0.49	3.80	0.12	2.25	--	--	--	4.92
N10	74.59	1.09	9.22	0.14	1.59	0.00	0.00	0.00	13.37

The N_2 adsorption-desorption isotherms for the AC series are compiled in Figure 1. For all the samples type I isotherms with a sharp increase of N_2 adsorption at low relative pressures are obtained. This pattern means a general microporous structure for all the ACs but it can also be observed that adsorption capacity within a given series is strongly influenced by the number of cycles applied.
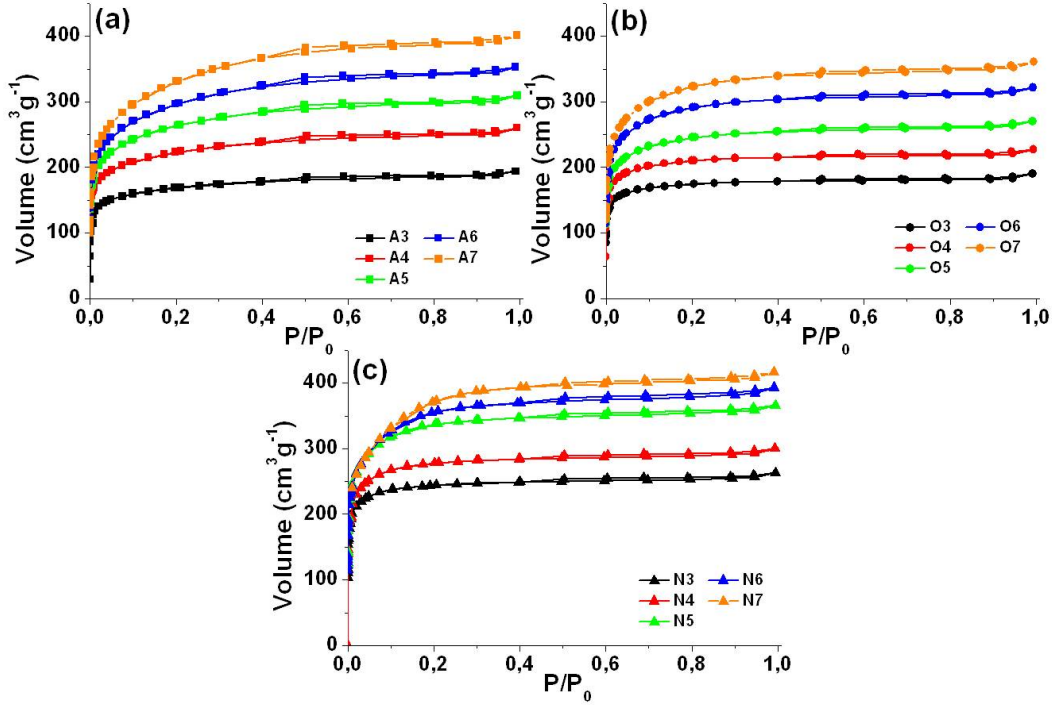
Figure 1.N2 adsorption-desorption isotherms for carbons activated with (a) air, (b) ozone and (c) HNO3.

The use of the different oxidants affects all the aspects of porous texture of the ACs, as evidenced by the textural parameters calculated from N_2 and CO_2 isotherms (Table 2). The starting char used in this work was mainly microporous, with a S_{BET} of $47m^2g^{-1}$ and a S_{DA} of $505m^2g^{-1}$ [18]. For the three experimental series, the samples showed a constant increase in surface area along the activation cycles, both in S_{BET} and in S_{DA}. S_{BET} results were similar for the series oxidized in gas phase (1124 and $1121m^2g^{-1}$ for air and ozone, respectively, after seven activation cycles applied), while oxidation with HNO_3 led to higher porosity development ($1354m^2g^{-1}$of S_{BET} after seven activation cycles). However, differences between gas-phase oxidants become significant for S_{DA}, with values of 1260 and $1524m^2g^{-1}$ for air and ozone respectively, after the whole cycles series. As a general conclusion it is possible to say that the porosity development with air and nitric acid is similar in terms of both S_{BET} and S_{DA} (slightly higher using nitric

acid) while higher S_{DA} than S_{BET} can be achieved when ozone is used as oxidizing agent.

Table 2. Textural parameters of char and the ACs.

Sample	S_{BET} (m^2g^{-1})	S_{DA} (m^2g^{-1})	L_0 (nm)	V_{mesoN2} (cm^3g^{-1})	$V_{microN2}$ (cm^3g^{-1})	$V_{microCO2}$ (cm^3g^{-1})	$V_{microN2}/$ V_T
Char	47	505	0.64	0.006	0.018	0.174	0.75
A3	594	668	0.89	0.028	0.261	0.254	0.90
A4	786	868	0.93	0.043	0.344	0.350	0.89
A5	937	1021	1.20	0.051	0.413	0.432	0.89
A6	1061	1127	1.39	0.063	0.467	0.494	0.88
A7	1124	1260	1.48	0.081	0.498	0.582	0.86
O3	614	790	0.76	0.012	0.269	0.312	0.96
O4	741	947	0.78	0.021	0.328	0.385	0.94
O5	840	1066	0.92	0.027	0.378	0.454	0.93
O6	1004	1297	1.13	0.034	0.449	0.579	0.93
O7	1121	1524	1.17	0.041	0.499	0.704	0.92
N3	857	1056	0.89	0.020	0.337	0.429	0.94
N4	981	1111	1.00	0.025	0.424	0.462	0.94
N5	1205	1239	1.15	0.035	0.515	0.559	0.94
N6	1240	1296	1.21	0.050	0.540	0.570	0.92
N7	1354	1309	1.30	0.047	0.581	0.583	0.93

The results of specific surface area discussed above are in concordance with the values obtained for the average micropore width (L_0), which increased along the cycles for all the experimental conditions tested. Those series that showed the highest S_{DA} values, which means higher development of narrow microporosity, also showed the lowest L_0 (1.17, 1.30 and 1.48nm for ozone, nitric acid and air respectively) after seven activation cycles. The air oxidation led to the widest dispersion of pore sizes. However, the narrowest range of average micropore width is achieved in ozone oxidation.

The simultaneous increase of micro and mesoporosity that can be deduced from S_{BET} and S_{DA} results discussed above was corroborated attending the monotonical increase of

the volume of mesopores and micropores (V_{mesoN2}, $V_{microN2}$ and $V_{microCO2}$) for the three experimental series. However, this increase does not occur to the same extent for meso and micropores and is different in each series of materials, so it depends on the oxidizing agent used, especially the mesopore volume. While $V_{microN2}$ increases 48, 46 and 42% for series treated with air, ozone and nitric acid respectively, the V_{mesoN2} increases 65, 71 and 58%. Therefore, the increase is much higher for mesopore volume than for micropore volume. The contribution of microposity, calculated as $V_{microN2}/V_T$ ratio, is presented in Table 2. In the case of air activation this ratio decreases from 0.90 to 0.86 as the number of activation cycles increases in along the activation, indicating a higher development of mesoporosity, in agreement with the higher L_0 values. The $V_{microN2}/V_T$ ratio remains in a narrower range for the activation with ozone and nitric acid (0.96 and 0.92). This fact can be explained by a higher enlarging of micropores and the pore wall destruction as a result of gasification [25, 26] in the case of air activation, although thermal stress can also induce a collapse of the microporous structure leading to the formation of mainly mesopores [27].

This observation can be also supported by the pore size distribution results obtained from the N_2 and CO_2 adsorption isotherms by the NLDFT method (Figure 2). In this figure, the results of PSD for three selected samples with similar S_{BET} (900-1000m^2g^{-1}) are compared (A5, O6 and N4). The three samples show very similar PSD in the ultramicropore region (between 0.4 and 0.9nm) with peaks at 0.45, 0.55 and 0.88nm. This may suggests that the ultramicropore structure is not conditioned by the preparation conditions but predetermined by the char. However, from the NLDFT distribution calculated from N_2 isotherm (pore diameter higher than 1nm) some differences between the samples can be seen, although the distribution profiles are centered in a narrow mesopore range (1.5 to 6nm) for all samples. N4 sample has the

narrowest distribution, centered at 1.8nm, followed by O6, centered at 2nm, and the A5 have the widest PSD, centered at 2.1nm. Finally, no significant differences can be found in the pattern of mesoporosity in the 8-50 nm range, probably because this porosity was present in the starting char.
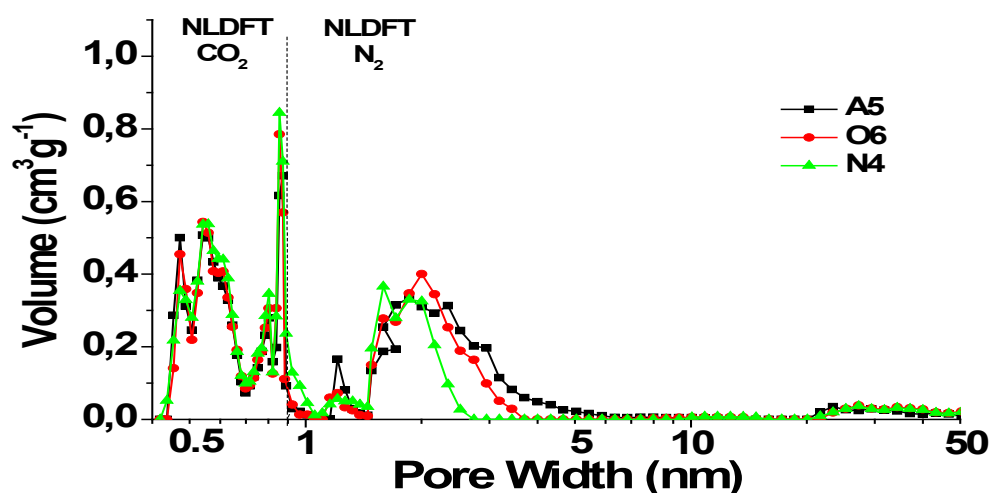

Figure 2. Pore size distribution by the NLDFT method from N_2 and CO_2 isotherms for selected samples (S_{BET} between 900-1000m^2g^{-1}).

Figure 3 summarizes the evolution of the textural properties along the activation cycles for the different oxidant agents, showing that the most effective method for developing specific surface area in a lower number of cycles is the activation with HNO_3. Figure 3 also shows that air and ozone activation result in similar surface area, but air activation develops both ultramicroporosity ($V_{microCO2}$) and microporosity ($V_{microN2}$), whereas ozone oxidation results in materials with more ultramicroporous character.
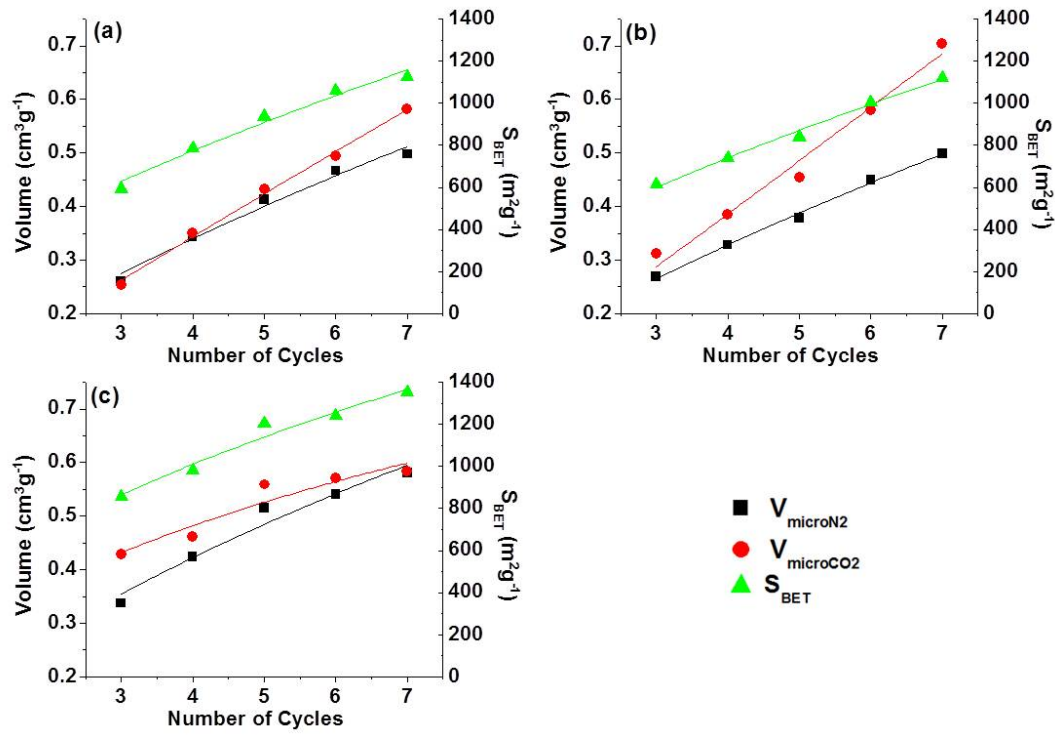
13

Figure 3. Micropore volume and BET surface area versus number of cycle for (a) air, (b) ozone and (c) HNO$_3$ series.

Figure 4 shows S$_{BET}$ plotted versus the average pore size (L$_0$) for the three series of porous materials, it can be observed that samples activated with air are characterized by higher pore size for a given S$_{BET}$, whereas the activation with HNO$_3$ leads to narrower porosity and higher S$_{BET}$. This means that air oxidation gives rise to a more important widening of the porosity along activation cycles, followed by ozone and HNO$_3$.
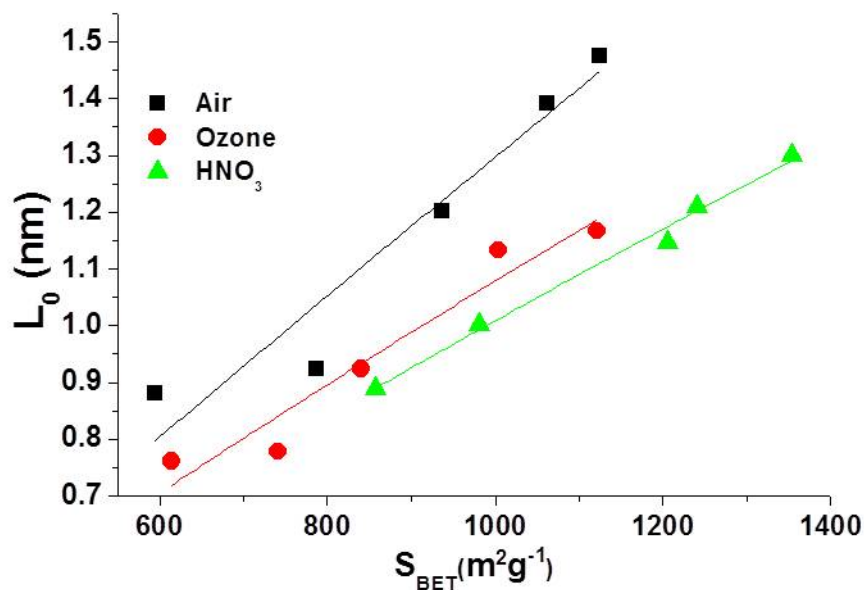
14

Figure 4. Average pore size versus BET surface area.

To summarize, by an adequate selection of operating conditions (oxidation procedure and number of cycles) it is possible to develop different pore structures (volume and pore size distribution) of AC. According with the characteristics of the materials prepared, they are very good candidates for studying the influence of carbon textural properties on the electrochemical behavior of carbon-carbon symmetric supercapacitors operating in different aqueous electrolytes.

3.2. Electrochemical characterization

The AC materialswere characterized at first as electrodes in symmetric two electrode capacitors by cyclic voltammetry (CV), using a voltage range from 0.6 to 2.0V for Na_2SO_4 and from 0.6 to 1.4V for KOH and H_2SO_4 at a constant rate of $2mVs^{-1}$ and by galvanostatic charge/discharge at a constant current density of $200mAg^{-1}$. Figure 5 shows the plots of data acquired by these techniques for the O5 sample in Na_2SO_4 as a representative example (for the rest of the samples very similar diagrams were

obtained). The CV curves exhibit a typical capacitor behaviour showing a nearly rectangular shape for cell voltages up to 1.0V. For higher cell voltages, the deviation from the rectangular shape is related to pseudocapacitive reversible reactions taking place at the positive and the negative electrode, i.e., fast redox reactions between the oxygen surface functionalities and the electrolyte at the positive electrode, and redox reactions related to the reversible electrosorption of hydrogen at the negative one [28]. In the same direction, galvanostatic charge/discharge curves demonstrate a pure capacitive behaviour, with straight lines, at cell voltages up to 1.0V. For values higher than 1.0V, there is a distortion fromlinearity associated to the above mentioned pseudo-capacitive effects.
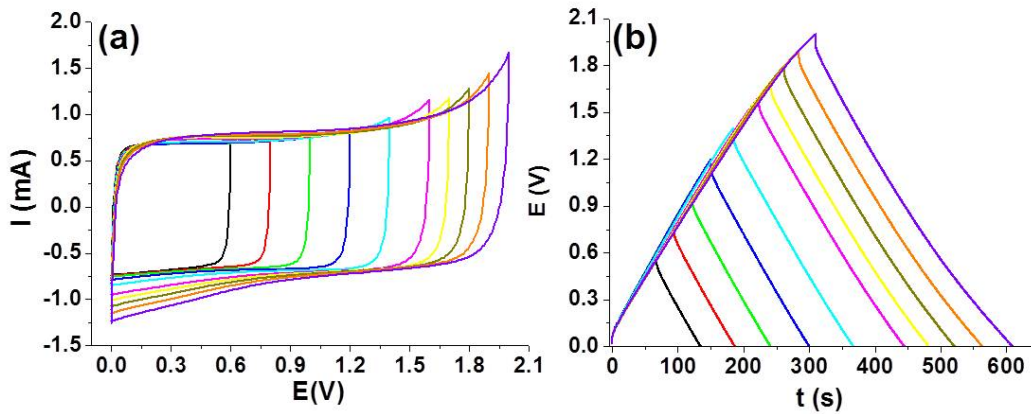

Figure 5. (a) Cyclic voltammetry with charge rate $2mVs^{-1}$ and (b)galvanostatic charge/discharge with a current density $200mAg^{-1}$ in Na_2SO_4 for O5 sample.

These experiments allowed selecting the optimum operating voltages for each electrolyte to be used in the further characterization of the samples. In particular, this maximum operating cell voltage has been determined from the coulombic efficiency (calculated as the ratio between the discharge and charge times obtained from the galvanostatic charge/discharge) considering that a supercapacitor normally operates at

values higher than 98% [29]. The voltages chosen were 1.8V for Na_2SO_4, 0.8V for KOH and 1.0V for H_2SO_4.

The gravimetric capacitance (C) values calculated by galvanostatic charge/discharge at the maximum cell voltage for each electrolyte, plotted versus the S_{BET} for the three series of ACs are shown in Figure 6. In general, the lowest values of capacitance are obtained using Na_2SO_4 as electrolyte while H_2SO_4 gave the highest results. These differences can be explained due to the difference in conductivity of the electrolyte solutions, i.e., 80, 800 and 1000mScm^{-1} for Na_2SO_4, KOH and H_2SO_4 respectively. For Na_2SO_4 and KOH solutions as electrolytes, no dependence of capacitance from a specific surface area is observed in the results presented in Figure 6. However, in the case of H_2SO_4 solution, there is an increase of the capacitance when increasing S_{BET} for all the AC series. The last is the expected behaviour and the reasons for not obtaining the same in Na_2SO_4 and KOH solutions are probably also related to conductivity.

Moreover, it seems that the effect of the surface functionality on the capacitance is not very relevant. Although the N-series possess the poorest surface functionality (see Table 1), it displays the higher capacitances. In particular, such effect is observed in the acid media (Figure 6c), where the most important pseudo-capacitive effect of the surface functionalities could be expected [1].
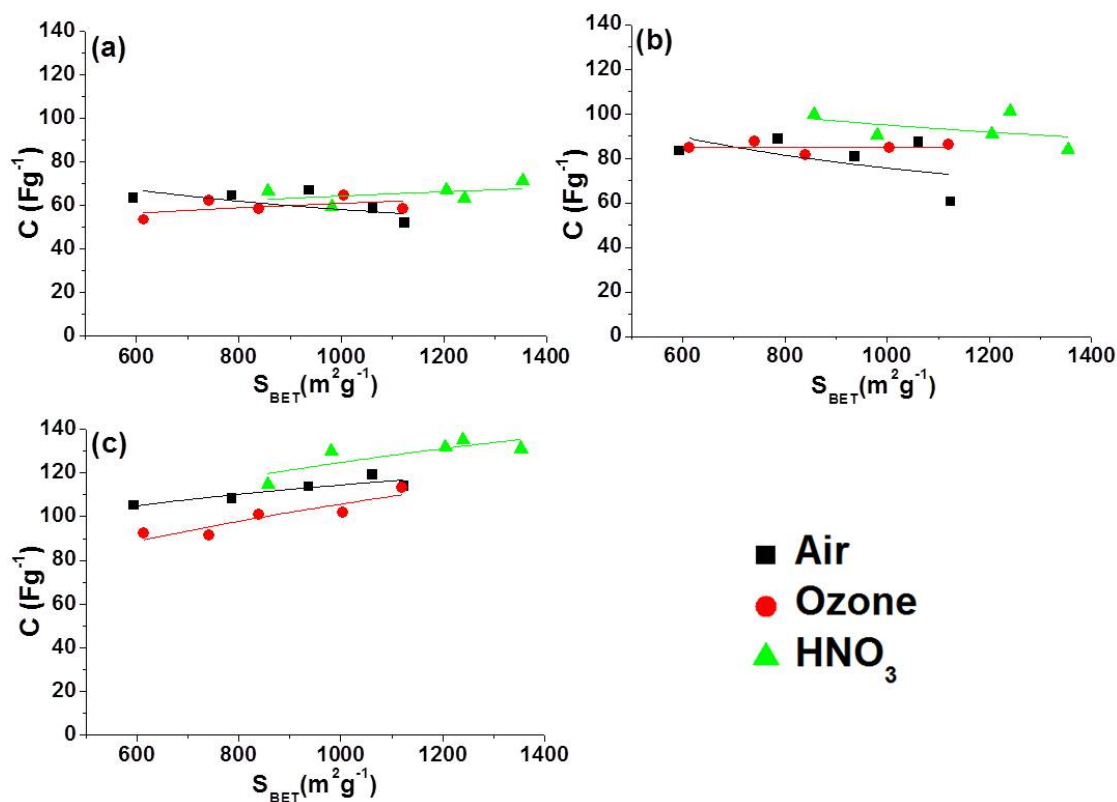
Figure 6. Gravimetric capacitance of the three series of ACs vs.specific surface area (results obtained by galvanostatic charge/discharge at 200mAg^{-1} with a voltage of (a) 1.8V in 1molL^{-1} Na$_2$SO$_4$, (b) 0.8V in 6molL^{-1} KOH and (c) 1.0V in 1molL^{-1} H$_2$SO$_4$).

In order to explore the effect of the electrolyte conductivity on the electrochemical performance, impedance spectroscopy has been performed over the grape seeds carbon based supercapacitors in all the electrolytes. Table 3 collects the ESR results which are obtained from the high frequency limit (10kHz) of the impedance spectrum and is related to the sum of the ohmic resistances of the electrode materials, contacts and electrolyte.

18

Table 3. Electrical series resistance for the three series of ACs.

Sample	ESR (Ω)		
	Na$_2$SO$_4$	KOH	H$_2$SO$_4$
A3	1.473	0.721	0.728
A4	1.507	0.604	0.509
A5	1.342	0.632	0.510
A6	1.776	0.655	0.482
A7	1.208	0.579	0.571
O3	1.084	0.426	0.701
O4	1.125	0.915	0.728
O5	1.549	0.537	0.473
O6	1.363	0.708	0.633
O7	1.344	0.726	0.523
N3	1.415	0.694	0.439
N4	1.454	0.636	0.471
N5	1.368	0.671	0.537
N6	1.486	0.525	0.452
N7	1.245	0.528	0.490

The table shows that ESR values, regardless the carbon material, in each electrolyte follow the inverse trend to their conductivity i.e. ESR$_{Na2SO4}$> ESR$_{KOH}$> ESR$_{H2SO4}$. Moreover, the ESR does not depend on the electrode material as for each electrolyte the values are nearly constant. Hence, the porous texture variations through the activation cycles do not modify the conductivity of the carbon material.

From the impedance spectroscopy we can also extract the EDR, which is mainly related to the diffusion of ions into the charge storing material and is obtained from the so-called Nyquist plots (representing the real part of the resistance versus the imaginary one) by extrapolating the nearly linear low frequency region down to the real part axis.

Figure 7 shows that EDR depends on the electrolyte used and on the micropore volume of the carbon electrode material. For a highly conductive electrolyte such as H_2SO_4 there is almost no relationship between the EDR and the micropore volume, indicating that the ions easily diffuse into the micropores whatever their size. However when the electrolyte is less conductive, as for KOH or Na_2SO_4, an increase of the resistance is observed when the micropore volume increases. Such effect is more visible for the less conductive electrolyte, i.e. Na_2SO_4, indicating that there is a kinetic barrier for the ions diffusing into the micropores when the mobility of the ions in the electrolyte is low. Moreover, the fact that this effect is more marked for the HNO_3 series is related with (i) the higher microporosity developed in comparison to the other two carbon series (see Figure 3) and (ii) the smaller amount of oxygen surface functionalities (see Table 2) and hence to the worst wettability of the carbon electrode surface. Therefore, the increase of EDR vs micropore volume observed when using Na_2SO_4 or KOH as electrolyte is not observed for H_2SO_4, which is related to the increase of the ions diffusion resistance to penetrate the pores in such media when developing the surface and the micropore volume.
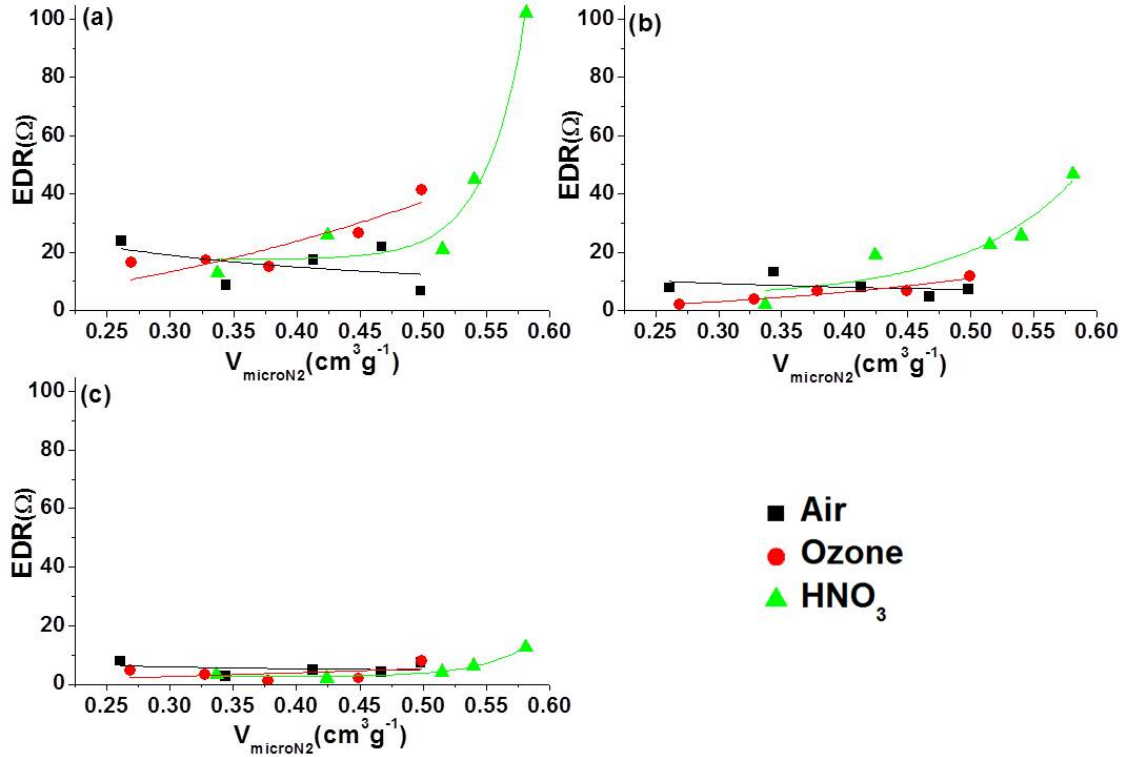
Figure 7. EDR results obtained by impedance spectroscopy of the three series of ACs vs. micropore volume in the three electrolytes: (a) Na_2SO_4, (b) KOH and (c) H_2SO_4.

In addition, when using H_2SO_4 as electrolyte, where kinetic effects do not much apply, Figure 6 shows that the three series of carbon follow the same ascendant trend of C vs S_{BET},but capacitance values are slightly different. The fact that the gravimetric capacitance values for the same value of surface area follow the order HNO_3>Air>Ozone series is related to their different textural properties. Firstly, HNO_3 series present higher amount of micropores for accommodating the charges than the other two series (Figure 3). Secondly, the series of ACs prepared by activation with air and ozone were compared. For the air series the micropore volume values obtained by N_2 and CO_2 adsorption are close. On the contrary, in the series of ACs obtained using ozone the micropore volume obtained by CO_2 adsorption is larger than that obtained by N_2 adsorption. Such results indicate that for the ozone series the micropores are narrower than for the air one [30], as is also confirmed by the smaller L_0 values

21

calculated for the ozone series (see Figure 4). Therefore, the small size of the micropores for the ozone series could induce a kind of ion sieving which could explain whythe gravimetric capacitances are smaller here than for the air series.

In order to better assess the effect of the porous texture on the electrochemical performance of porous carbons in aqueous electrolytes, Figure 8 presents the specific capacitance (Cs) as a function of the average pore size (L$_0$) obtained in the three electrolytes at different current densities. For small current densities (200 mAg^{-1}) the known trend in which the specific capacitance increases for average pore sizes smaller than 1 nm [3, 6] is obtained independently of the electrolyte used for the supercapacitors built with all the carbon series. Such results confirm that the double layer is more efficiently formed in pores of this size [3, 6]. Moreover, the less effective character of larger pores versus the double layer formation is reflected on the decrease of the Cs when increasing L$_0$. The differences observed in Cs within a carbon series for the same electrolyte are related to the differences in porous texture already discussed above.

However, keeping in mind that supercapacitors are power devices, it is necessary to explore the electrochemical behaviour during fast charging, i.e., at high current densities. Actually, previous studies regarding the effect of the pore size on the electrochemical performance did not deeply analyse such aspect as the results are usually presented for small or moderate current densities [3-7].

Figure 8 shows that by increasing the current density the Cs vs L$_0$ becomes a straight line when Na$_2$SO$_4$ is used as electrolyte, while at small current densities the trends are the same found for KOH and H$_2$SO$_4$. Such results are in concordance to the EDR results presented in Figure 7. In fact, the diffusion of ions inside the micropores is kinetically unfavourable when the conductivity of electrolyte solution is low, as in the case of

Na$_2$SO$_4$. This effect is more visible when the charge-discharge of the supercapacitor is faster. Therefore, for electrolytes as Na$_2$SO$_4$, small micropores have an enhancing effect on the capacitance for low current densities but they have a negative effect on the capacitance when increasing the current density. This is also the reason why the current density has the most detrimental effect on the capacitance of the carbon materials of the ozone series in reason of their smaller micropores size.
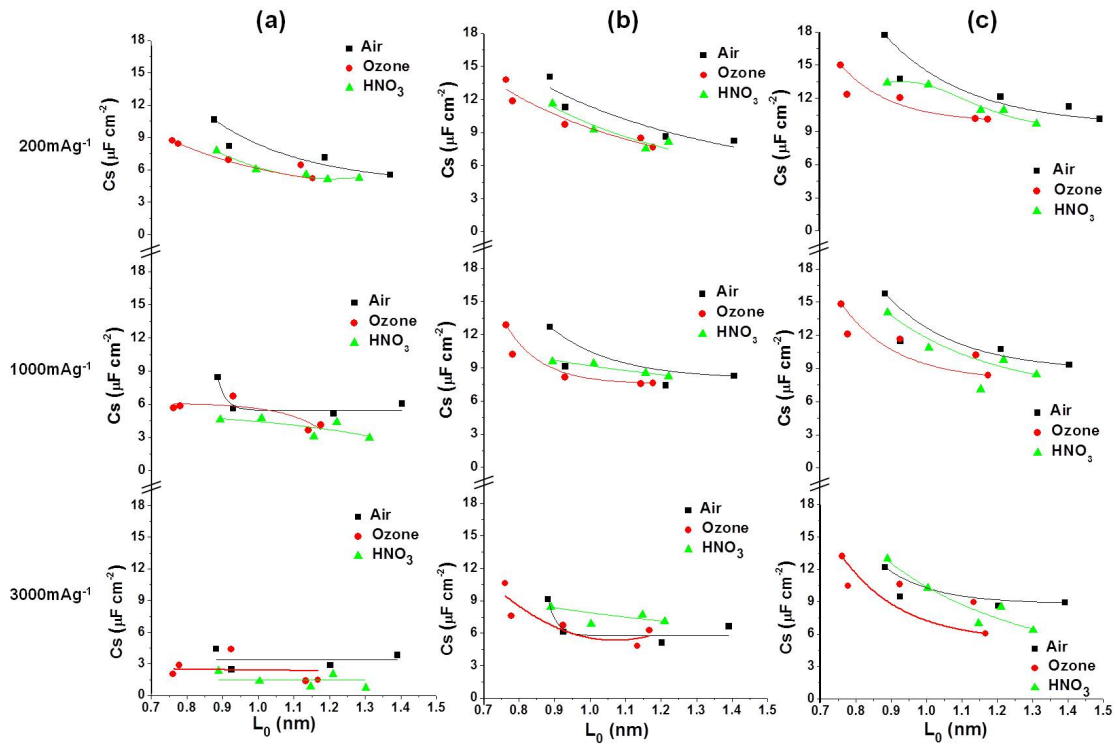

Figure 8. Specific capacitance vs L$_0$ at different current densities in the electrolytes (a) Na$_2$SO$_4$, (b) KOH and (c) H$_2$SO$_4$.

In the same direction, if the capacitance retention (expressed as the percentage of the capacitance obtained at low current densities) is plotted versus the current density for samples of different series having a similar specific surface area (A5, O6 and N4, ~1000 m^{2}g^{-1}, see Figure 9), it can be observed that the most pronounced capacitance loss is always obtained when using Na$_2$SO$_4$ as electrolyte. Moreover, the results presented in Figure 9 confirm that a narrow microporosity can be a disadvantage when operating at

23

high current densities in a poorly conductive electrolyte as Na_2SO_4. In particular, the differences between electrolytes are more marked for the N4 carbon having a smaller average pore size (1.0 nm) than for the sample A5 having a wider one (1.2 nm), even if they have the same specific surface area.

Therefore, although energy density can be improved using neutral electrolytes in reason of their higher stability potential window than the acidic or basic ones, it is important to adapt the porous texture of the carbon material for improving the ions diffusion inside the porosity for assuring the charging of the double layer at high current densities to attain high power densities.
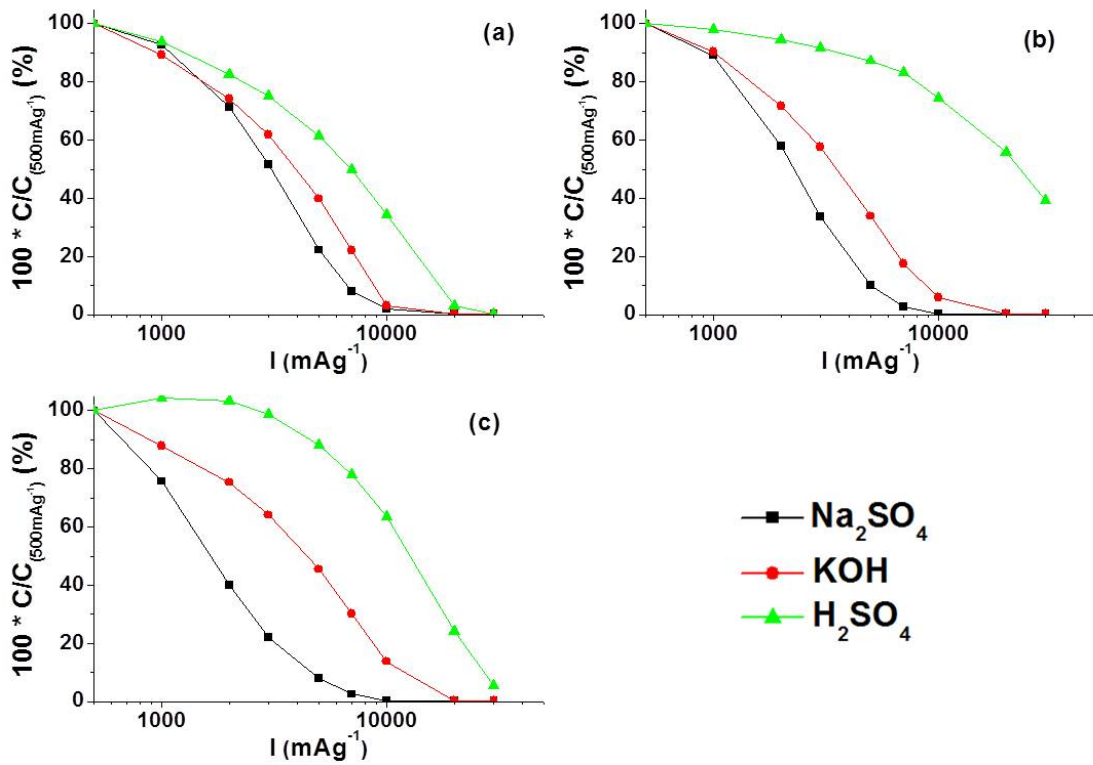

Figure 9. Capacitance vs current density plots obtained by galvanostatic charge/discharge with a voltage 1.8V in Na_2SO_4, 0.8V in KOH and1.0V in H_2SO_4 for ACs (a) A5, (b) O6 and (c) N4.

In this sense Figure 10 depicts the Ragone plots for the supercapacitors built with the three samples of different series having similar specific surface areas but different average pore sizes. It is clear that for small powers, corresponding to small current densities and high discharge times, the energy density is always higher in Na_2SO_4 independently of the porous texture of the electrode active material in reason of the higher cell voltage. For the same reasons, the electrolyte with lower performance is always KOH because of the low cell voltage that can be used. Such differences are more visible when using the carbon samples with smaller average pore size, i.e. N4, as electrode material. In fact, higher values of maximum extractable energy (E_{max}) can be obtained for the N4 based supercapacitor than for the A5 one in Na_2SO_4. However, for small discharge time ranging between 10s and 1s, which is usually the operation range for a supercapacitor, the advantages of using the high stability potential window of Na_2SO_4 are not visible anymore. In particular, Figure 10 shows that for the N4 based supercapacitor the extractable energy at a given power is now smaller in Na_2SO_4 than in H_2SO_4 as electrolyte. For the N4 supercapacitor, only 36% of the maximum energy is retained at 10s discharge time in Na_2SO_4, whereas 94% is done in H_2SO_4. Contrarily, for the A5 based supercapacitor, having a smaller E_{max} in Na_2SO_4 than N4, 65% of this energy can be kept at 10s.Therefore higher energy and power densities can be extracted at small discharge times for the A5 supercapacitor than for the N4 one. Moreover, contrarily to the N4 supercapacitor, the A5 one present more important energy density values at 10s discharge time in Na_2SO_4 than in H_2SO_4.

Hence, for taking profit of all the advantages of a non-corrosive, high energy potential window electrolyte as Na_2SO_4, it is necessary to use carbon materials having a micropore size narrow enough to ensure the efficiency of the double layer formation for giving high energy densities but not too narrow in order to avoid diffusion problems of

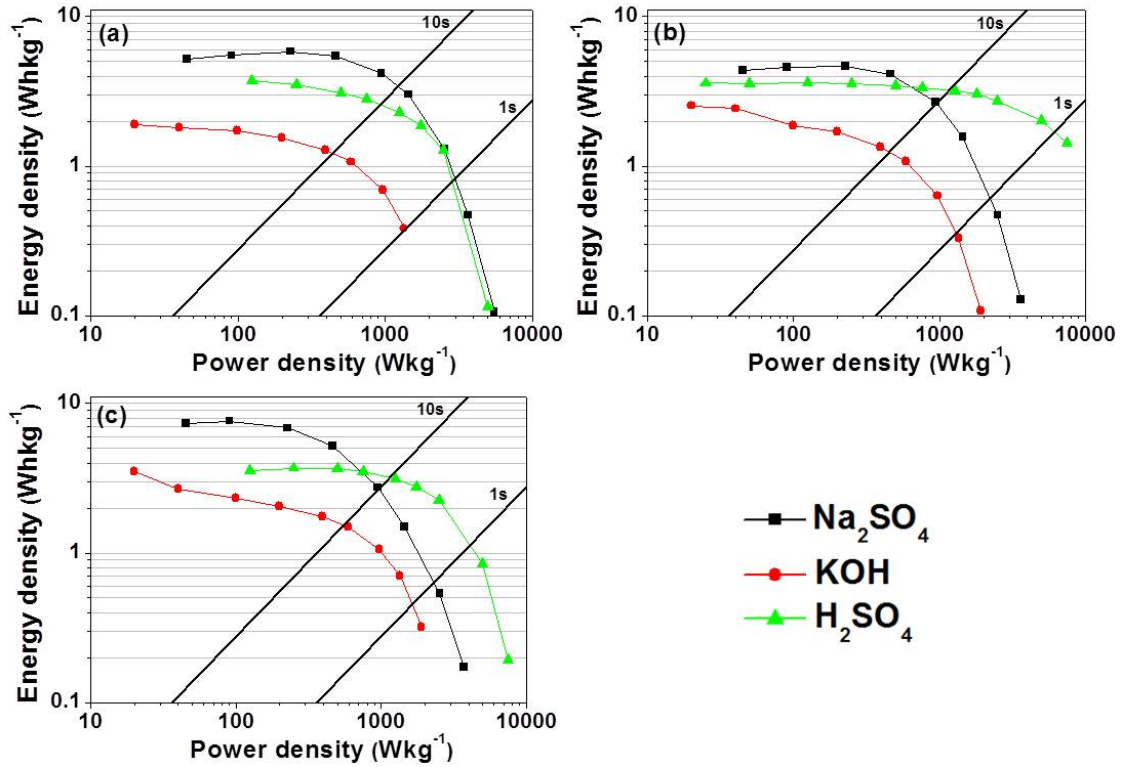such a poor conductive electrolyte inside the porosity and to keep enough energy at high power densities.

Figure 10. Ragone plot for supercapacitors operating in Na_2SO_4, KOH and H_2SO_4 using as electrode active material (a) A5, (b) O6 and (c) N4.

4. Conclusions

In this study, microporous carbon materials having a negligible contribution of mesopores have been synthesized by cyclic oxidation/desorption of grape seeds char using air, ozone and HNO_3 as oxidant agents. It has been shown that the pore structure of the thereof produced carbons depends on the oxidant agent used. In particular, the most effective method for developing specific surface area using the smaller number of cycles is the HNO_3 based one.Air and ozone activation results in similar surface areas

26

along the activation cycles, although air activation develops ultramicroporosity and microporosity in the same extent and ozone oxidation leads to materials with more ultramicroporous character. As a consequence, in terms of average pore size, air oxidation drives to a more important widening of the porosity than ozone activation and even more than HNO_3 activation. Therefore, by an adequate selection of operating conditions (oxidation procedure and number of cycles) it is possible to tune the volume and pore size distribution of ACs and the influence of carbon textural properties on the electrochemical behavior of carbon-carbon symmetric supercapacitors operating in different aqueous electrolytes can be determined.

By comparing the electrochemical performance of the three series of carbons in a neutral, basic and acidic electrolyte (Na_2SO_4, 6 $molL^{-1}$ KOH and 1 $molL^{-1}$ H_2SO_4) it has been shown that the gravimetric capacitance for a same electrode active material follows the trend of the electrolyte conductivity, i.e., the highest values are obtained in H_2SO_4 and the lowest are shown in Na_2SO_4. Moreover, the relationship between the gravimetric capacitance and the textural parameters of the electrode material is also mastered by conductivity issues. In fact, when the conductivity of the electrolyte is decreased there is an increase of the ions diffusion resistance to penetrate the micropores. As a consequence, increasing of the specific surface area and of the micropore volume have a positive effect on the capacitance, mainly when using the electrolyte with the highest conductivity (H_2SO_4).

Regarding the effect of the pore size on the electrochemical performance, it has been shown that for small current densities the known trend in which the specific capacitance increases for average pore sizes smaller than 1 nm is obtained independently of the electrolyte used for the supercapacitors built with all the carbon series. Such results confirm that the double layer is more efficiently formed in pores of this size. However,

when increasing current densities, such small pore sizes have a negative effect on the capacitance if a poorly conductive electrolyte such as Na_2SO_4 is used. Consequently, for small powers the energy density is always higher in Na_2SO_4 than in the acidic or basic electrolyte independently of the porous texture of the electrode active material in reason of the higher cell voltages. However, for taking profit of all the advantages of a non-corrosive, high energy potential window electrolyte as Na_2SO_4 it is necessary to adapt the porous texture of the carbon material with micropore sizes large enough to improve the ions diffusion inside the porosity and attain high power densities.

5. Acknowledgments

6. References

[1] Andreas H.A., Conway B.E. Examination of the double-layer capacitance of an high specific area C-cloth electrode as titrated from acidic to alkaline pHs. Electro.Acta2006; 51(28): 6510–20.

[2] Mysyk R., Raymundo-Piñero E., Pernak J., Béguin F. Confinement of Symmetric Tetraalkylammonium Ions in Nanoporous Carbon Electrodes of Electric Double-Layer Capacitors. J. Phys. Chem. 2009; 113(30): 13443–9.

[3] Raymundo-Piñero E., Kierzek K., Machnikowski J., Béguin F. Relationship between the nanoporous texture of activated carbons and their capacitance properties in different electrolytes. Carbon 2006; 44(12): 2498–507.

[4] Ra E.J., Raymundo-Piñero E., Lee Y.H., Béguin F. High power supercapacitors using polyacrylonitrile-based carbon nanofiber paper. Carbon 2009; 47(13): 2984–92.

[5] Li X., Xing W., Zhuo S., Zhou J., Li F., Qiao S-Z., et al. Preparation of capacitors electrode from sunflower seed shell.Bioresource Technology 2011; 102(2): 1118 – 23.

[6]Chmiola, J.; Yushin, G.; Gogotsi, Y.; Portet, C.; Simon, P.; Taberna, P.L. Anomalous Increase in Carbon Capacitance at Pore Sizes Less Than 1 Nanometer. Science 2006; 313(5794): 1760–3.

[7]Guo Y., Qi J., Jiang Y., Yang S., Wang Z., Xu H. Performance of electrical double layer capacitors with porous carbons derived from rice husk. Mater.Chem. Phys.2003; 80(3): 704–9.

[8] Yang, J., Liu, Y., Chen, X., Hu, Z., Zhao, G. Carbon electrode material with high densities of energy and power. Acta Physica-ChimicaSinica2008; 24(1): 13–9.

[9]Markoulidis F., Lei C., Lekakou C., Duff D., Khalil S., Martorana B., et al. A method to increase the energy density of supercapacitor cells by the addition of multiwall carbon nanotubes into activated carbon electrodes. Carbon 2013; http://dx.doi.org/10.1016/j.carbon.2013.08.040

[10]Demarconnay L., Raymundo-Piñero E., Béguin F. A symmetric carbon/carbon supercapacitor operating at 1.6 V by using a neutral aqueous solution. Electrochem. Commun. 2010; 12(10): 1275–8.

[11] Gao Q., Demarconnay L., Raymundo-Piñero E., Béguin F. Exploring the large voltage range of carbon/carbon supercapacitors in aqueous lithium sulfate electrolyte. Energy Environ. Sci. 2012; 5(11): 9611–7.

[12]Fic K., Lota G., Meller M., Frackowiak E. Novel insight into neutral medium as electrolyte for high-voltage supercapacitors. Energy Environ. Sci. 2012; 5(2): 5842–50.

[13]Barbieri O., Hahn M., Herzog A., Kötz R. Capacitance limits of high surface area activated carbons for double layer capacitors. Carbon 2005; 43(6): 1303–10.

[14] Heras F., Alonso-Morales N., Jiménez-Cordero D., Gilarranz M. A., Rodríguez J. J. Granular mesoporous activated carbons from waste tires by cyclic oxygen chemisorption-desorption. Ind. Eng. Chem. Res.2012; 51(6): 2609–14.

[15] Jiménez-Cordero D., Heras F., Alonso-Morales N., Gilarranz M.A., Rodríguez J.J. Development of porosity upon physical activation of grape seeds char by gas phase oxygen chemisorption-desorption cycles. Chem.Eng. J.2013; 231: 172–81.

[16] F. Heras, N. Alonso-Morales, M.A. Gilarranz, J.J. Rodríguez. Activation of waste tire char upon cyclic oxygen chemisorption-desorption. Ind. Eng. Chem. Res. 2009; 48(10): 4664–70.

[17]Solís-Fernández, P., Paredes J.I., Cosío A., Martínez-Alonso A., Tascón J.M.D. A comparison between physically and chemically driven etching in the oxidation of graphite surfaces. J. Colloid Interface Sci.2010; 344(2): 451–9.

[18] Jiménez-Cordero D., Heras F., Alonso-Morales N., Gilarranz M.A., Rodríguez J.J. Porous structure and morphology of granular chars from flash and conventional pyrolysis of grape seeds. Biomass Bioenergy. 2013; 54: 123–32.

[19] Jiménez-Cordero D., Heras F., Alonso-Morales N., Gilarranz M.A., Rodríguez J.J. Gas phase oxidation with ozone for the preparation of granular activated carbons from grape seeds by cyclic oxidation-desorption. Waste Management. Submitted (2013).

[20] Jiménez-Cordero D., Heras F., Alonso-Morales N., Gilarranz M.A., Rodríguez J.J. Preparation of granular activated carbons from grape seeds by cyclesof liquid phase oxidation and thermal desorption. Fuel Process. Technol. 2014; 118: 148–55.

[21] Brunauer S., Emmett E., Teller E. Adsorption of gases in multimolecular layers. Am. Chem. Soc. J.1938; 60: 309–19.

[22] Gil A., Grange P. Application of the Dubinin-Radushkevich and Dubinin-Astakhov equations in the characterization of microporous solids. Colloid Surf. A: Physicochem. Eng. Aspects 1996; 113(1-2): 39–50.

[23] Jagiello J., Thommes M. Comparison of DFT characterization methods based on N_2, Ar, CO_2 and H_2 adsorption applied to carbons with various pore size distributions. Carbon 2004; 42(7): 1227–32.

[24]Stoeckli F., Daguerre E., Guillot A. The development of micropore volumes and widths during physical activation of various precursors. Carbon 1999; 37(12) 2075–7.

[25] Sing K.S.W., Everett D.H., Haul R.A.W., Moscou L., Pierotti R.A., Rouquerol J., et al. Reporting physisorption data for gas/solid systems with special reference to the determination of surface area and porosity. Pure Appl. Chem. 1985; 57(4): 603–19.

[26] Álvarez P.M., García-Araya J.F., Beltrán F.J., Masa F.J., Medina F. Ozonation of activated carbons: Effect on the adsorption of selected phenolic compounds from aqueous solutions. J. Colloid Interface Sci.2005; 283(2): 503–12.

[27] Raymundo-Piñero E., Béguin F. Interface science and technology, Volume 7. Chapter 6: Aplication of nanotextured carbons for supercapaciitors and hydrogen storage. Academic Press; 2006, p. 293-308.

[28]Béguin F., Raymundo-Piñero E, Frackowiak E. Carbons for electrochemical energy storage and conversion systems. Chapter 8: Electrical double-layer capacitors and pseudocapacitors. CRC Press; 2010, p. 334.

[29] http://www.maxwell.com.

[30]Cazorla Amorós, D.; Alcañiz Monge, J.; de la Casa Lillo, M. A.;. Linares Solano, A. CO_2 as an adsorptive to characterize carbon molecular sieves and activated carbons. Langmuir 1998; 14(16): 4589–96.

7. Figure Captions

Figure 1. N_2 adsorption-desorption isotherms for carbons activated with (a) air, (b) ozone and (c) HNO_3.

Figure 2. Pore size distribution by the NLDFT method from N_2 and CO_2 isotherms for selected samples (S_{BET} between 900-1000m^2g^{-1}).

Figure 3. Micropore volume and BET surface area versus number of cycle for (a) air, (b) ozone and (c) HNO_3 series.

Figure 4. Average pore size versus BET surface area.

Figure 5. (a) Cyclic voltammetry with charge rate 2mVs^{-1} and (b)galvanostatic charge/discharge with a current density 200mAg^{-1} in Na_2SO_4 for O5 sample.

Figure 6. Gravimetric capacitance of the three series of ACs vs. specific surface area. The results were obtained by galvanostatic charge/discharge at 200mAg^{-1} with a voltage of (a) 1.8V in 1$molL^{-1}$ Na_2SO_4, (b) 0.8V in 6$molL^{-1}$ KOH and (c) 1.0V in 1$molL^{-1}$ H_2SO_4.

Figure 7. EDR results obtained by impedance spectroscopy of the three series of ACs vs. micropore volume in the three electrolytes: (a) Na_2SO_4, (b) KOH and (c) H_2SO_4.

Figure 8. Specific capacitance vs L_0 at different current densities in the electrolytes (a) Na_2SO_4, (b) KOH and (c) H_2SO_4.

Figure 9. Capacitance vs current density plots obtained by galvanostatic charge/discharge with a voltage 1.8V in Na_2SO_4, 0.8V in KOH and 1.0V in H_2SO_4 for ACs (a) A5, (b) O6 and (c) N4.

Figure 10. Ragone plot for supercapacitors operating in Na_2SO_4, KOH and H_2SO_4 using as electrode active material (a) A5, (b) O6 and (c) N4.

8. Table Captions

Table 1. Composition of ACs obtained by activation with air, ozone and HNO_3 after 1, 4, 7 and 10 activation cycles.

Table 2. Textural parameters of the ACs.

Table 3. Electrical series resistance for the three series of ACs.